SPECTROPHOTOMETRY AND IMAGING OF AGN FROM 2.5 TO 11.6 MICRON

B. Schulz, J. Clavel, B. Altieri,
P. Barr, P. Claes, A.M. Heras, K. Leech, L. Metcalfe, A. Salama

ISO Data Centre, ESA Astrophysics Division, Villafranca del Castillo, Spain.

ABSTRACT

We present low resolution spectrophotometric and imaging ISO observations of a sample of 58 AGN's over the 2.5–11.6 μm range. The data strongly support unification schemes and set new constraints on models of the molecular torus.

Key words: AGN, Seyfert Galaxies, Infrared, Spectroscopy.

1. INTRODUCTION

According to the "unified model" of Active Galactic Nuclei (AGN), Seyfert 1 and Seyfert 2 galaxies (hereafter Sf1 and Sf2) are the same objects viewed at a different angle: Sf1's are observed close to face-on such that we have a direct view to the Broad emission Line Region (BLR) and the accretion disk responsible for the strong UV-Optical-X-ray continuum, whereas Sf2's are seen at an inclination such that our view is blocked by an optically thick dusty torus which surrounds the disk and the BLR (e.g. Antonucci 1993). This model makes specific predictions. In particular, the UV photons from the disk which are absorbed by the grains in the torus should be re-emitted as thermal radiation in the IR. Several arguments constrain the torus inner radius to be of the order of $\sim$ 1 pc in which case the dust temperature should peak to about 700–1000 K and give rise to an emission "bump" between$\simeq$ 2 and 15 μm (Pier & Krolik 1992). The model also predicts that the silicate 9.7 μm feature should appear preferentially in absorption in Sf2's and in emission in Sf1's. In order to test these predictions and better constrain the model, we initiated a programme of mid-IR observations of a large sample of AGN's. Throughout we use $H_0 = 75\,\mathrm{km\,s^{-1}}$; $q_0 = 0$.

2. OBSERVATIONS

A sample of 57 AGN and one non active "normal" SB galaxy was observed with the PHT and CAM instruments on board the Infrared Space Observatory (ISO; Kessler et al. 1996). The sample is drawn from the CfA hard X-ray flux limited complete sample but lacks the most well known objects (e.g. NGC 4151) which were embargoed by ISO guaranteed time owners. On the other hand, the sample was enriched in bright Sf2's. We caution that our sample is therefore not "complete" in a statistical sense. It is about equally divided into Sf1's (28 sources, including 2 QSO's) and Sf2's (29), where we define Sf1's as all objects of type $\leq$ 1.5 and Sf2's those whose type is $>$ 1.5. The mean and *r.m.s.* redshift are 0.047 ± 0.083 and 0.016 ± 0.013 for Sf1's and Sf2's.

For each object, the data-set consists of CAM images obtained through filters at 6.75 and 9.63 μm, together with 2.5–11.6 μm spectra obtained immediately before with the PHT-S low resolution ($3000\,\mathrm{km\,s^{-1}}$) spectrograph. The images consist of arrays of 32×32 pixels (i.e. 96×96 arcsec) with an effective resolution (FWHM) of 3.8 and 4.5 arcsec, for the 6.75 and 9.63 μm filters, respectively. The exposure times were 200 s, sufficiently long to ensure stabilisation of the detectors. For the spectra, on-source measurements were alternated with sky measurements at a frequency of 1/256 Hz, with a chopper throw of 300 arcsec. The on-source exposure times varied between 512 s and 2048 s, depending on the source brightness. The spectrograph aperture is 24×24 arcsec^2.

3. CALIBRATION AND DATA REDUCTION

The CAM images were reduced and calibrated using standard procedures of the CAM Interactive Analysis (CIA) package. Nuclear fluxes were obtained by integrating all the emission in a circle of 5–6 pixels radius (15–18 arcsec). Their accuracy, mainly limited by flat-fielding residuals, is $\pm$10 per cent. Radial profiles were also computed and compared to that of point-like calibration stars. For all sources but 4, the AGN are unresolved at the $\simeq$ 4 arcsec resolution of ISOCAM. Because PHT-S was operating close to its sensitivity limit, special reduction and calibration procedures had to be applied. After a change of illumination, the responsivity of the Si:Ga photoconductors immediately jumps to an intermediate level. This initial jump is followed by a characteristic slow transient to the final level. At the faint flux limit, this time constant is extremely long, and in practice only the initial step is observed in chopped-mode. The spectral response function for this particular mode and flux-level was derived directly from ob-

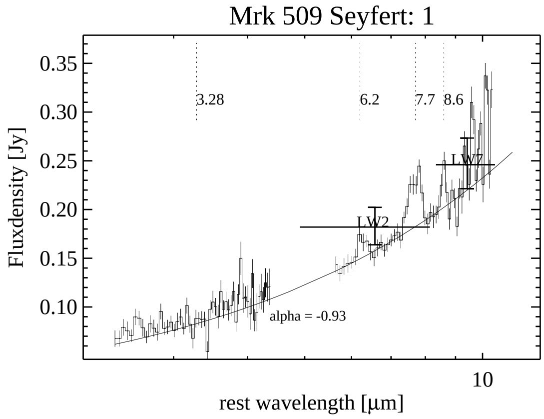

Figure 1. A representative Sf1 spectrum with error bars. The two data-points marked LW2 and LW7 indicate the flux from the CAM images with its error and the filter wavelength range. The best-fit power-law continuum is also shown.

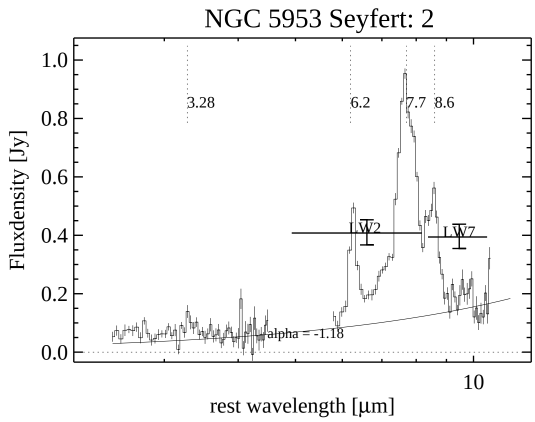

Figure 2. A representative Sf2 spectrum.

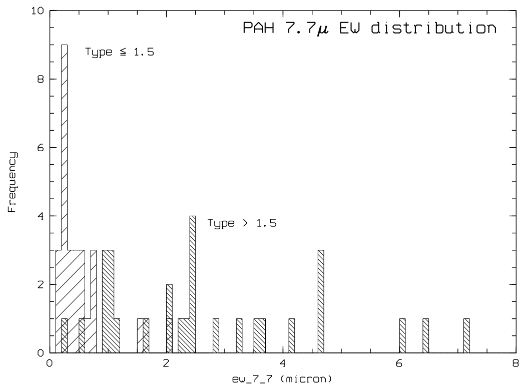

Figure 3. Distribution of PAH 7.7 μm EW for Sf1 (spaced hatching at +45 deg*) & Sf2 (fine hatching, -45* deg*).*

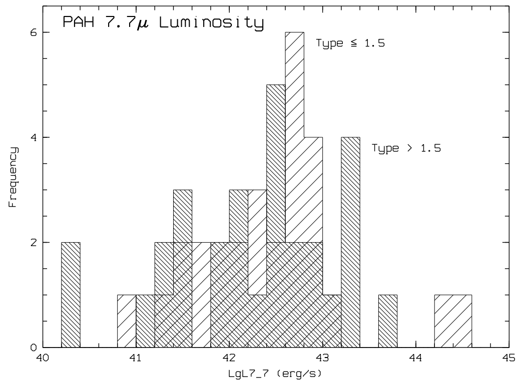

Figure 4. Distribution of PAH 7.7 μm luminosities for Sf1 (spaced hatching at +45 deg*) & Sf2 (fine hatching, -45* deg*).*

servations of a faint standard star HD 132142 whose flux ranges from 0.15 to 2.54 Jy. The calibration star observation was performed with the same chopper frequency and readout-timing as the AGN observations. The S/N of the PHT-S spectra was considerably enhanced by two additional measures: *i)* the 32-s integration ramps were divided into sub-ramps of 2 sec and no de-glitching (removal of cosmic ray hits) was performed at ramp-level *ii)* after slope-fitting and de-glitching at slope-level, the maximum of the distribution of the slopes was determined by fitting a gaussian to the histogram. The resulting PHT-S fluxes should be accurate to within ±10 per cent.

For all sources but 4, the agreement between the CAM and the PHT-S flux is excellent which confirms the reliability of our calibration. The 4 slight mismatches occur for the 4 spatially resolved sources.

4. THE DIFFERENCE BETWEEN SF1 AND SF2

As illustrated in Figure 1, the mid-IR spectrum of a typical Sf1 (Mrk 509) is markedly different from that of a Sf2 (NGC 5953, Figure 2): Sf1's have a strong continuum well approximated by a power-law ($F_\nu \propto \nu^\alpha$) of average index and *r.m.s.* dispersion $\langle\alpha\rangle = -0.84 \pm 0.24$ and weak emission features. By contrast, most Sf2's display only a weak continuum together with very strong emission features. These features have well defined peaks at at 6.2, 7.7 and 8.6 μm, usually ascribed to Polycyclic Aromatic Hydrocarbon (PAH) bands. In many galaxies of adequate S/N and redshift, the blue side of the strong 11.3 μm PAH feature is also detected as a sharp rise in flux toward the long wavelength end of the PHT-S array (see e.g. Figure 7). The mean spectral index of the Sf2's, $\langle\alpha\rangle = -0.75 \pm 0.56$ is consistent with that of Sf1's. The EW distribution of the strongest PAH band at 7.7 μm is shown in Figure 3. It clearly illustrates that PAH's are systematically weaker in Sf1's than in Sf2's where

EW's extend up to $\sim$ 7 μm. A two-tail KS test confirms that Sf1's and Sf2's have statistically different EW distributions at the $4 \cdot 10^{-8}$ confidence level. The mean ($\pm r.m.s$) 7.7 μm PAH equivalent width of Sf1's is $\langle \mathrm{EW_{PAH}} \rangle = 0.53 \pm 0.47\,\mu$m, 5 times smaller than that of Sf2's, $\langle \mathrm{EW_{PAH}} \rangle = 2.72 \pm 1.83\,\mu$m. As can be seen from Figure 4, the distribution of the 7.7 μm PAH *luminosity* is however the same in Sf1's and Sf2's, at the 52 per cent confidence level (KS test). The mean ($\pm r.m.s$) PAH luminosity of Sf1's is $\langle \log \mathrm{L_{PAH}} \rangle = 42.44 \pm 0.80$ erg s^{-1}, not statistically different (at the 26 per cent confidence level) from that of Sf2's, $\langle \log \mathrm{L_{PAH}} \rangle = 42.22 \pm 0.87$ erg s^{-1}.

5. IMPLICATION FOR UNIFICATION SCHEMES

The continuum flux at a fiducial wavelength of 7 μm was read-out from the best-fit power-law. The resulting mean ($\pm r.m.s.$) continuum logarithmic luminosities for Sf1's and Sf2's are $\langle \log \nu\, \mathrm{L}_{\nu,7} \rangle = 43.73 \pm 0.86$ and 42.80 ± 0.79 erg s^{-1}, respectively, implying that the mid-IR continuum of Sf2's is $\sim$ 9 times less luminous, on the average, than that of Sf1's. Together with the difference in PAH EWs, these results imply that *the prime distinguishing feature of Sf2's in the mid-IR is that their continuum is depressed relative to that of Sf1's.*

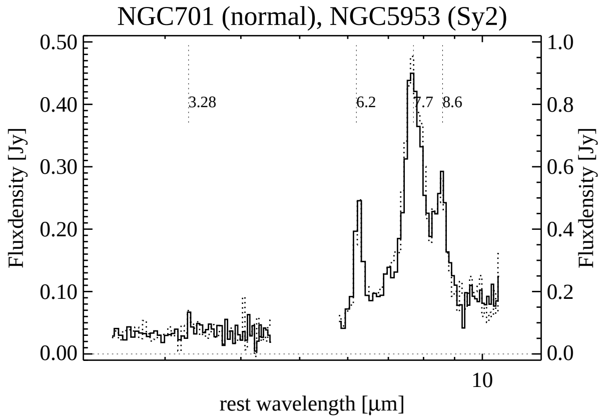

Figure 5. The spectra of the non-active galaxy NGC 701 (heavy line) and of the Sf2 galaxy NGC 5953 (dotted-line).

The above result is broadly consistent with unification schemes as illustrated in Figure 6, where the mid-IR continuum, which is directly visible in face-on objects (i.e. Sf1's), is largely extinguished in edge-on objects (i.e. Sf2's). It further implies that the torus is opaque to its own mid-IR radiation. Assuming that face-on objects suffer zero extinction, one can use the average PAH EW ratio $\langle R \rangle$ in Sf1's and Sf2's to infer the mean Sf2 extinction. The average ratio for the strongest PAH band at 7.7 μm is $\langle R \rangle = 5.2 \pm 3.5$, where the error quoted reflects the r.m.s. dispersion of Sf2 EW's. This implies that the Sf2 continuum suffers on the average from 1.8 ± 0.7 magnitudes of extinction at 7.7 μm, i.e. $\mathrm{A_v} = 89 \pm 37$ magnitudes

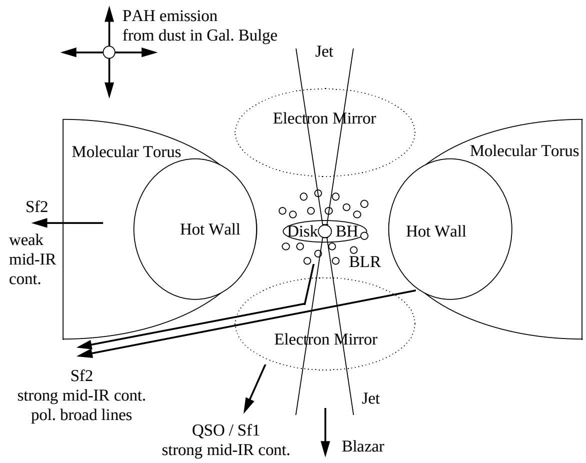

Figure 6. A graphical illustration of a unification scheme for Seyferts. Sf1 types are seen face-on, Sf2 types are seen edge-on. Sf2 types with "hidden" BLR are seen at a grazing angle. The PAH emission is not related to the AGN.

(Rieke & Lebofsky 1985). For a normal gas to dust ratio, this corresponds to an average X-ray absorbing column, $\mathrm{N_H} = 2.0 \pm 0.8 \cdot 10^{23}$ cm^{-2} (Gorenstein 1975). The latter is in good agreement with the mean Sf2 absorbing column as measured directly from X-ray data by Mulchaey, Mushotzky & Weaver (1992), $\mathrm{N_H} = 1.6^{+8.6}_{-1.3} \cdot 10^{23}$ cm^{-2} or Smith & Done (1996), $\mathrm{N_H} = 1.0 \pm 1.3 \cdot 10^{23}$ cm^{-2}. The large dispersion in $\mathrm{A_v}$ and $\mathrm{N_H}$ presumably reflects the spread in Sf2 torus viewing angles, i.e. from grazing incidence to completely edge-on.

It also suggests that PAH emission is isotropic and arises from outside the torus, either in the Narrow Line Region or in the ISM of the bulge. To check the origin of the PAH features, we have observed the nucleus of the "normal" (i.e. non active) SB galaxy NGC 701. Its PHT-S spectrum is plotted in Figure 5 together with that of the Sf2 nucleus NGC 5953. The mid-IR spectrum of NGC 701 – fairly typical of a "normal" galaxy (Helou et al. 1998) – is virtually indistinguishable from that of NGC 5953. As a matter of fact, the 7.7 μm PAH EW in NGC 701, $5.88 \pm 0.05\,\mu$m and luminosity, $\log \mathrm{L_{PAH}} = 42.048 \pm 0.009$ erg s^{-1}, are well within the range spanned by Sf2's. We therefore conclude that the *PAH emission is unrelated to the active nucleus and arise from the ISM in the bulge.*

As can be seen from Figure 5, also the continuum of NGC 5953 is indistinguishable from that of NGC 701. This further suggests that in Sf2's with 7.7 μm PAH EW's in excess of $\simeq 5\,\mu$m, the torus emission is totally suppressed, at least up to 11.6 μm, and the faint residual mid-IR continuum arises entirely from outside the active nucleus, i.e. from stars shortward of $\sim 3\,\mu$m and from very small ISM dust particles at longer wavelengths. In such objects, the PAH EW only provides a lower limit to $\mathrm{A_v}$ and $\mathrm{N_H}$. From the 29 Sf2's, only 3 have $\mathrm{EW_{PAH}} \geq 5\,\mu$m. This suggests that about 10 per cent of Sf2's suffer from extinction in excess of 125 visual magnitudes, sufficient to block-

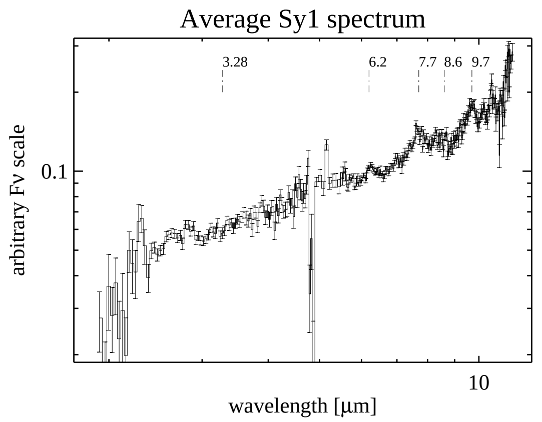

Figure 7. The average Sf1 spectrum of the 28 type ≤ 1.5 galaxies in the sample.

out the mid-IR continuum. These extreme Sf2's are presumably those where the torus symmetry axis lies in the plane of the sky.

Ten Sf2 galaxies have $7.7\,\mu$m PAH EW $\leq 1.6\ \mu$m, in the range occupied by Sf1's (Figure 3). Among these, four have been observed in spectropolarimetry and *all 4 display broad-lines in polarized light*. These are Mrk 3, NGC 7674, IRAS 05189-2524 and NGC 4388 (Heisler et al. 1996). Conversely, none of the three Sf2's with $7.7\,\mu$m PAH EW $> 1.6\ \mu$m for which spectropolarimetric or IR spectroscopic data exist (Mrk 266, NGC 5728, NGC 1097) have "hidden" broad lines. This confirms the suggestion by Heisler et al. that those Sf2 which have "hidden" BLR (seen in spectropolarimetry or in direct IR spectroscopy) are those for which our line of sight (LOS) grazes the torus upper surface such that we can see the reflecting mirror but not the BLR. The mid-IR continuum most likely originates from thermal emission by hot dust grains located on the inner wall of the torus. Hence, the fact that the "hidden" BLR Sf2's are the same sources which display a Sf1-like mid-IR continuum further constrains the mirror and the torus inner wall to be in neighbouring regions. It is conceivable that the mirror is the wall itself or a wind of hot electrons boiled-off the torus. Mrk 3 has an X-ray absorbing column of $10^{24}\,\mathrm{cm}^{-2}$ (Turner et al. 1997) corresponding to an extinction of 125 magnitudes, sufficient to block the mid-IR radiation. The fact that it is nevertheless visible up to $11.6\,\mu$m indicate that the X-ray source is embedded further down the throat of the torus than the mirror and the wall emitting the mid-IR continuum.

6. THE SILICATE $9.7\,\mu$m FEATURES AND FURTHER CONSTRAINTS ON THE TORUS

Figure 7 shows the weighted mean Sf1 spectrum obtained by averaging the rest wavelength spectra of all 28 type ≤ 1.5 AGN's. The Silicate $9.7\,\mu$m feature appears *in emission* with an equivalent width $\langle \mathrm{EW}_{9.7} \rangle = 0.254 \pm 0.009\,\mu$m. This immediately *rules out models with very large torus optical depths.* In the model of Pier & Krolik (1992) for instance, the strength of the Silicate feature is calculated as a function of inclination i and of the vertical and radial Thomson optical depth τ_z and τ_r, respectively. Reading from their Figure 8, models with $\tau_z \geq 1$ and/or $\tau_r \geq 1$ are ruled-out as they would predict the Silicate feature in absorption. For an average Sf1 inclination $\cos i = 0.8$, the best fit to $\langle \mathrm{EW}_{9.7} \rangle = 0.254 \pm 0.008\,\mu$m suggests $\tau_r \simeq 1$ and $0.1 \leq \tau_z \leq 1$. A unit Thomson optical depth corresponds to a column density $\mathrm{N_H} \simeq 10^{24}\,\mathrm{cm}^{-2}$. While these figures are somewhat model dependent, it is reassuring that they agree with our independent estimate of $\mathrm{N_H}$ based on the PAH EW ratio. The PAH bands are so strong in Sf2's that placing the continuum at $9.7\,\mu$m becomes a subjective decision. The mean Sf2 spectrum shows a weak maximum at $9.7\,\mu$m and a shallow minimum near 10 μm. In the absence of longer wavelengths data, one can only set a provisional upper limit of $0.32\,\mu$m to the Silicate EW in Sf2's, whether in absorption or in emission.

7. BIBLIOGRAPHIC REFERENCES

REFERENCES

Antonucci, R. 1993, ARAA., 31, 473

Gorenstein, P. 1975, ApJ, 198, 95

Helou, G. et al. 1998, preprint

Heisler, C.A. et al. 1996, Nature, 385, 20

Kessler, M.F., Steinz, J.A., Anderegg, M.E., et al. 1996, A&A, 315, L27

Mulchaey, J.S., Mushotzky, R.F. & Weaver, K.A. 1992, ApJ, 390, L69

Oliva, E. et al 1998, A&A 329, 210

Pier, E.A. & Krolik, J.H. 1992, ApJ, 401, 99

Rieke, G.H. & Lebofski, M.J. 1985, ApJ, 288, 618

Roche, P.F. et al. 1991, MNRAS, 248, 606.

Smith, D.A. and Done, C. 1996, MNRAS, 280, 355

Turner, T.J. et al 1997, ApJ 488, 164